PHOTONICS Research

Bright single-photon sources in the telecom band by deterministically coupling single quantum dots to a hybrid circular Bragg resonator

Shi-Wen Xu,† Yu-Ming Wei,† Rong-Bin Su, Xue-Shi Li, Pei-Nian Huang, Shun-Fa Liu, Xiao-Ying Huang, Ying Yu, Jin Liu,* and Xue-Hua Wang

State Key Laboratory of Optoelectronic Materials and Technologies, School of Physics, School of Electronics and Information Technology, Sun Yat-sen University, Guangzhou 510275, China
**Corresponding author: liujin23@mail.sysu.edu.cn*

Received 20 April 2022; revised 28 May 2022; accepted 5 June 2022; posted 6 June 2022 (Doc. ID 461034); published 21 July 2022

High-performance solid-state quantum sources in the telecom band are of paramount importance for long-distance quantum communications and the quantum Internet by taking advantage of a low-loss optical fiber network. Here, we demonstrate bright telecom-wavelength single-photon sources based on In(Ga)As/GaAs quantum dots (QDs) deterministically coupled to hybrid circular Bragg resonators (h-CBRs) by using a wide-field fluorescence imaging technique. The QD emissions are redshifted toward the telecom O-band by using an ultra-low InAs growth rate and an InGaAs strain reducing layer. Single-photon emissions under both continuous wave (CW) and pulsed operations are demonstrated, showing high brightness with count rates of 1.14 MHz and 0.34 MHz under saturation powers and single-photon purities of $g^{(2)}(0) = 0.11 \pm 0.02$ (CW) and $g^{(2)}(0) = 0.087 \pm 0.003$ (pulsed) at low excitation powers. A Purcell factor of 4.2 with a collection efficiency of 11.2% ± 1% at the first lens is extracted, suggesting efficient coupling between the QD and h-CBR. Our work contributes to the development of highly efficient single-photon sources in the telecom band for fiber-based quantum communication and future distributed quantum networks. © 2022 Chinese Laser Press

https://doi.org/10.1364/PRJ.461034

1. INTRODUCTION

Telecom-wavelength sources of single photons with high degrees of brightness, purity, and photon indistinguishability are highly desirable for long-distance quantum communication and distributed quantum networks, due to the low photon absorption and small dispersion in silica fibers. In the past decades, telecom-wavelength single-photon sources in a variety of material platforms have been extensively studied, such as atomic sources [1,2], optical nonlinear crystals [3,4], semiconductor quantum dots (QDs) [5–8], defects in silicon carbide [9,10], gallium nitride [11], and carbon nanotubes [12,13]. However, an on-demand telecom-wavelength source of single photons with simultaneous high degrees of brightness, single-photon purity, and photon indistinguishability is still illusive. Atomic ensembles have a long storage lifetime [14], which is good for quantum memory, but their low radiative rates ultimately restrict the brightness of the sources [15]. Spontaneous parametric downconversion (SPDC) sources based on optical nonlinear crystals can be operated at room temperature with high photon indistinguishabilities [16]. However, high single-photon purities can be obtained only with a probability typically <0.1 [17] under low excitation powers, which imposes an unavoidable trade-off between the source brightness and single-photon purity. Epitaxially grown semiconductor QDs have exhibited state-of-the-art performances as single-photon sources in the near-infrared regime with the assistance of photonic nanostructures such as micropillars [18–21], circular Bragg resonators (CBRs) [22–25], photonic crystals [26,27], and open microcavities [28]. Yet, transplanting high-performance single-photon sources based on QDs from near-infrared to telecom bands is still a highly nontrivial task. The difficulties lie on both the epitaxial growth and the deterministic couplings between the QDs and the photonic nanostructures. To redshift the emission wavelength, either the barrier materials for InGaAs QDs have to be modified [29,30] or low bandgap materials [31,32], e.g., InP, have to be employed in the growth. Recently, O-band single-photon emissions have been achieved in InGaAs QDs with a strain-reduced layer, and the first lens collection efficiency was improved to 23% [33] by using randomly coupled hybrid CBRs (h-CBRs). For InP QDs, O-band single-photon emission with first lens efficiencies of 36% and 27% [34,35] was reported in randomly coupled QD-photonic crystal systems. It is also shown that telecom emission QDs can be deterministically coupled to photonic nanostructures

via *in situ* electron beam (E-beam) lithography [36], while the achievable brightness can further be improved.

In this work, we present our efforts towards deterministically coupled QD single-photon sources in the telecom wavelength band by positioning single InGaAs QDs into an h-CBR via a wide-field fluorescence imaging technique [37,38]. A Purcell enhancement of 4.2 clearly reveals the efficient coupling between the QDs and h-CBR. We demonstrate an extraction efficiency of 11.2% ± 1% at the first lens with maximal photon count rates of 1.14 MHz and 0.34 MHz under CW (4.8 μW) and pulsed (5.4 μW) excitations, respectively. By lowering the excitation powers, better single-photon purities of $g^{(2)}(0) = 0.11 \pm 0.03$ and $g^{(2)}(0) = 0.087 \pm 0.003$ are obtained under CW (0.2 μW) and pulsed (1.1 μW) excitations, respectively.

2. EPITAXIAL GROWTH OF TELECOM BAND QDS

The samples were grown on semi-insulating GaAs (001) substrates in a solid-state molecular beam epitaxy (MBE) system equipped with a cracker cell for arsenic (As) evaporation and high-energy electron diffraction (RHEED). The deposition temperature was calibrated by the transition temperature T_c when the surface reconstruction pattern of GaAs transferred from 2×4 to 2×3 [39]. Figure 1(a) illustrates the growth layers. After deoxidization at a temperature of 680°C for 10 min and growth of 500 nm GaAs buffer at 660°C, a 250 nm $Al_{0.8}Ga_{0.2}As$ sacrificial layer was grown at 620°C, which is used for nanomembrane release [40]. The InAs QDs were embedded in the middle of a GaAs layer with a thickness of 240 nm. The emission range of the QDs is designed at 1310 nm (4 K) via capping an InGaAs strain-reduced layer on top of InAs QDs to minimize strain and surface energy. In detail, the InAs QD was deposited at a temperature of T_c – 25°C with an ultra-low indium flux rate of 0.004 mL/s and then capped with 8 nm $In_{0.17}Ga_{0.83}As$ and 5 nm GaAs, followed by a 3 min annealing step at 680°C. The morphology characterization of QDs was performed by an atomic force microscope (AFM, Bruker Icon, peak force tapping mode) using additional uncapped InAs QD deposition on GaAs with the same experimental parameters. Figure 1(b) shows the QD density of a few dots/μm^2 with an average height of 14–16 nm.

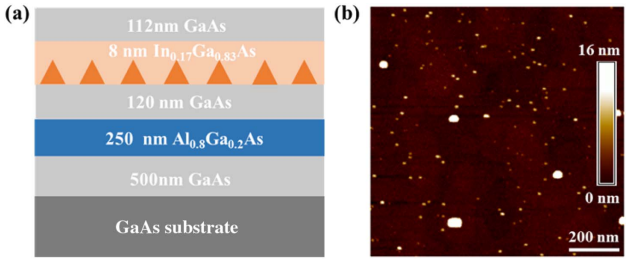

Fig. 1. Epitaxial growth of telecom band QDs. (a) Layer sequence of the investigated sample. (b) Representative AFM image of the QDs.

3. CBR DESIGN AND FABRICATION

The h-CBR studied in this work is schematically illustrated in Fig. 2(a), which consists of a circular GaAs disk surrounded by a set of concentric GaAs rings, placed on a highly efficient broadband Au reflector spaced with a 300-nm-thick SiO_2 layer [41,42]. A scanning electron microscope (SEM) image showing an exemplary CBR with the central disc diameter d of 585 nm is presented in Fig. 2(b). Figure 2(c) shows the calculated photon collection efficiency and Purcell factor by using finite-difference time-domain simulations (Lumerical FDTD solutions). For QD emission in a spectral range of 1321 to 1325 nm, the simulation displays a broadband out-coupling efficiency higher than 89.6% when collected from an object lens with a numerical aperture (NA) of 0.65. The far-field pattern of the cavity mode is shown in the inset of Fig. 2(c), in which most of the emitted light is confined in the divergence angle of 10°. The highest Purcell factor is 26.7, and Purcell enhancements of >5 can be readily achieved from 1321 nm to 1325 nm.

4. H-CBR DESIGN AND FABRICATION

A. Coupling between QD and CBR

The h-CBR devices were fabricated in three steps: (i) growing a 300 nm SiO_2 spacer layer and a 100-nm-thick Au reflector layer on top of the epitaxial wafer; (ii) transferring the III-V wafer on a quartz substrate and removing the GaAs substrate and AlGaAs sacrificial layer by using selective wet etching; (iii) defining CBR structures with electron beam lithography (EBL) and transferring the patterns from the E-beam resist into

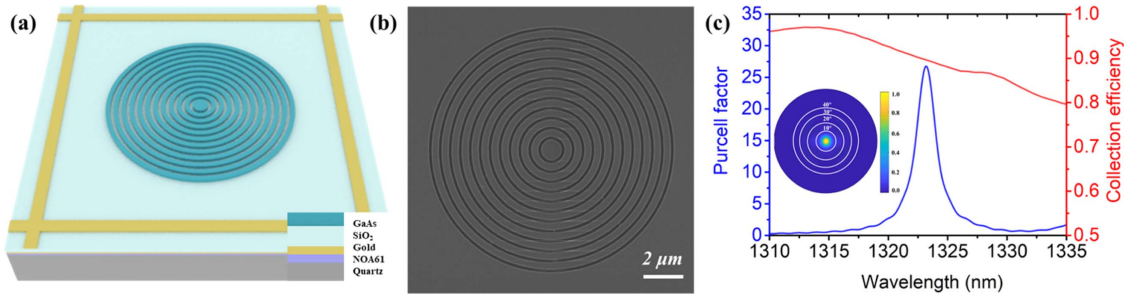

Fig. 2. h-CBR device for telecom band single-photon sources. (a) Schematic illustration of an h-CBR device. (b) Scanning electron micrograph of the fabricated h-CBR. (c) Simulated Purcell factor (blue) and collection efficiency (red) of the h-CBR as a function of wavelength. The collection efficiency is based on a 40° azimuth angle, corresponding to a lens with a numerical aperture (NA) of 0.65. The inset is the far-field intensity distribution of the cavity mode.

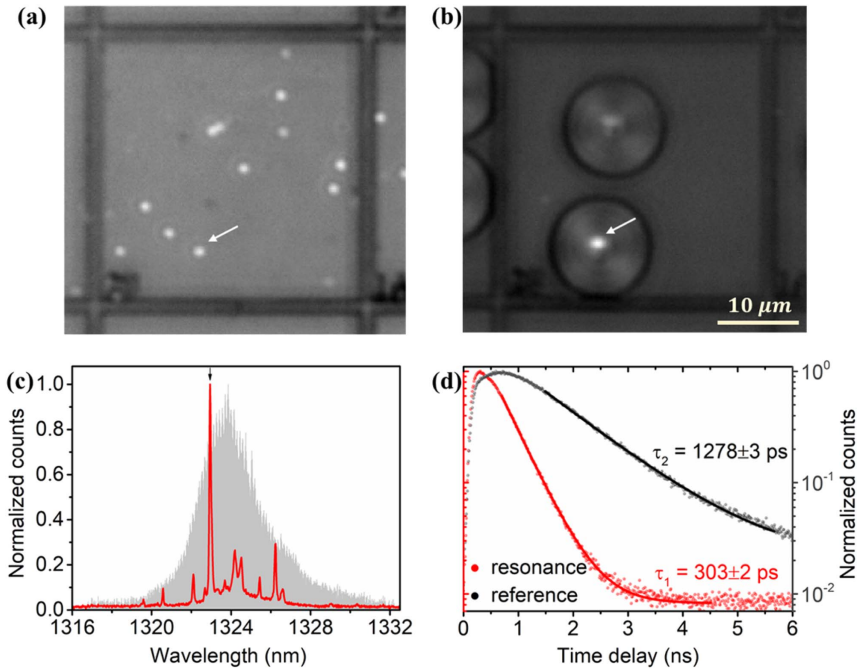

Fig. 3. Deterministically coupled QD-CBR device. Fluorescence images (34 μm × 34 μm) of the QDs (a) before and (b) after fabrication of the h-CBRs. (a) and (b) share the same scale bar. (c) Normalized micro-photoluminescence spectrum (red trace) and cavity mode (shaded area) under quasi-resonant (p-shell) excitation. The small black arrow denotes the investigated emission line at 1322.99 nm. (d) Lifetimes of the selected QD emission line (1322.99 nm) coupled with h-CBR (red point) and an exemplary reference QD outside the device (black point), indicating pronounced Purcell enhancement. Solid red and black lines are the exponential function fits.

the GaAs layer by using dry etching. To ensure spatial overlaps between the QDs and h-CBRs, we used a wide-field fluorescence imaging technique to extract the positions of QDs respective to the pre-fabricated alignment marks, as shown in Fig. 3(a). After fabrication of the h-CBRs, bright fluorescence spots were observed in the centers of the devices, indicating that the QDs are precisely placed in the centers of the h-CBRs, as presented in Fig. 3(b).

To optically characterize the deterministically coupled devices, a confocal micro-photoluminescence (μ-PL) setup is used. The sample was mounted inside a close-circle cryostat and cooled down to about 4 K. Then a pulsed laser (1150–2323 nm) with a repetition rate of 86 MHz and pulse width of 3 ps or a tunable CW diode laser (1240–1380 nm) was used to excite the QD via one of the excited states (p-shell) of the QDs. The PL signals were collected by a microscope objective with NA = 0.65 and detected by using an infrared spectrometer (spectral resolution ~0.06 nm). To perform time-resolved measurements, a home-built filter was used to select the targeted emission line before detecting the photons with fiber-coupled superconducting nanowire single-photon detectors (SNSPDs). More details are presented in the section. As shown in Fig. 3(c), a QD emission line (1322.99 nm) is almost resonant with the cavity mode (1323.87 nm) under pulsed p-shell excitation. The cavity mode is characterized by a full-width at half-maximum (FWHM) of 3.42 nm, corresponding to a Q-factor of 387. To further confirm the coupling between the QD and cavity mode, a Purcell enhancement of the transition is obtained by time-resolved measurements, as shown in Fig. 3(d). The Purcell factor is about 4.2 by comparing the lifetime of the coupled QD ($\tau_{\text{coupled}} = 303$ ps) with the lifetime of a reference QD outside the cavity ($\tau_{\text{outside}} = 1278$ ps). The deviation of the measured Purcell factor from the theoretical value could be from the uncertainties in the E-beam alignment process and the slight detuning between the emission line and the cavity mode.

B. Characteristic of Single-Photon Emission

We investigate the telecom band single-photon emission of our device operating under both CW and pulsed modes for different excitation powers. The single-photon purities of the emitted photons are extracted from the second-order correlations by using a fiber-based Hanbury Brown and Twiss setup. For low-excitation powers of 0.2 μW and 1.1 μW, both CW and pulsed emissions exhibit pronounced suppressions of coincidence events at zero delay, which gives rise to $g^{(2)}(0) = 0.11 \pm 0.02$ and 0.087 ± 0.003, respectively. The count rates of the emitted photons can be significantly improved with the sacrifice of single-photon purity by increasing the excitation power. At the saturation powers, we obtained $g^{(2)}(0)$ values of 0.38 ± 0.03 and 0.485 ± 0.003 under CW (4.8 μW) and pulsed (5.4 μW) excitations, respectively. The power dependences of the photon count rate and $g^{(2)}(0)$ value are plotted in Figs. 4(c) and 4(f) for CW and pulsed excitations, respectively, showing maximal photon count rates of 1.14 MHz and 0.34 MHz at the saturation powers. We note that blinking behaviors of the QDs on a time scale of around 13 ns and 0.5 ns are observed in Figs. 4(b) and 4(d).

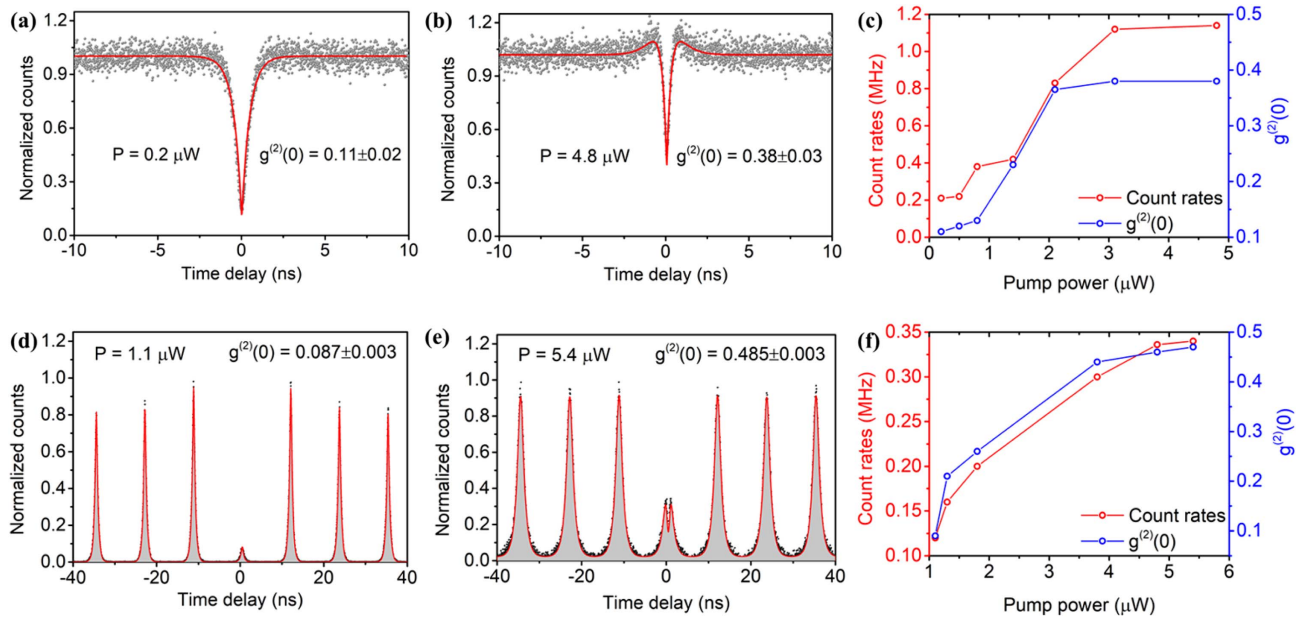

Fig. 4. Characterizations of the telecom band single-photon emissions. Autocorrelation measurements of single-photon emissions for (a) low-power (0.2 μW) and (b) high-power (4.8 μW) CW excitation. (c) Power dependences of the emission count rate and $g^{(2)}(0)$ value for CW excitation. Autocorrelation measurements of single-photon emissions for (d) low-power (1.1 μW) and (e) high-power (5.4 μW) pulsed excitation. (f) Power dependences of the emission count rate and $g^{(2)}(0)$ value for pulsed excitation.

The $g^{(2)}$ functions with blinking behaviors can be quantitatively fitted by introducing extra dark states in the model [43,44]. For low-power CW excitation, the blinking could be attributed to the nearby charge carrier and the physical defects on the sample surface. The carrier fluctuations in the vicinity of the QDs can shift the emission wavelength by the quantum-confined Stark effect [45] and cause nonradiative Auger recombination [46]. For high-power pulsed excitation, the nearby charge carrier traps can refill the QD, as reported in a previous study [33], as shown in Fig. 4(e).

Finally, the extraction efficiency of the device at the first lens is evaluated. Figure 5 shows the schematic of the experimental setup. The emitted photons are collected using a microscope objective with an NA of 0.65. For this measurement, the signals pass through a dichroscope and a beam splitter (BS) before coupling into a single-mode fiber. The emitted photons from the targeted emission line are selected by a home-built grating filter and detected by using fiber-coupled SNSPDs. More details are shown in the method section. The detection efficiency of the whole setup has been carefully calibrated to be 0.0238 ± 0.002 [see the table in Fig. 5(b)], leading to an extraction efficiency at the first lens of $16.6\% \pm 1.5\%$ at a saturation count rate of 0.34 MHz [Fig. 4(f)]. To remove the effect of re-excitation, we multiply a calibration factor with $1/(1+g^{(2)}(0))$ and get a corrected extraction efficiency of $11.2\% \pm 1\%$.

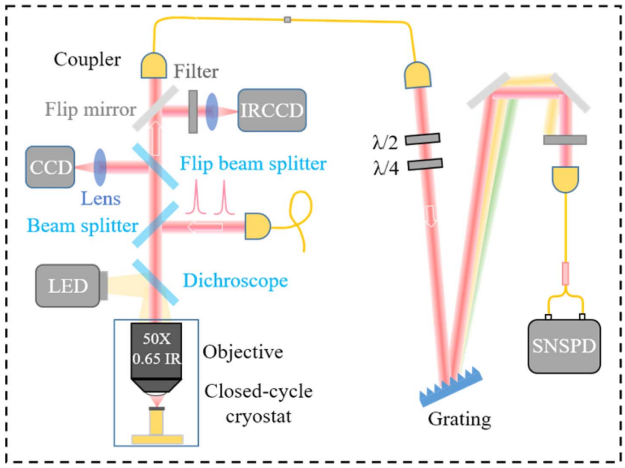

Optical setup	Efficiency
Glass	0.91
Objective	0.66
Dichroscope	0.87
Beam splitter	0.55
Fiber coupling efficiency	0.53
Silver mirrors	0.93
Filter setup	0.28
Fiber	0.75
SNSPD	0.80
Total	0.0238

Fig. 5. Estimation of the extraction efficiency at the first lens. Left: schematic of the experimental setup ($\lambda/2$, half-wave plate; $\lambda/4$, quarter-wave plate). Right table: transmissions of the optical elements used in efficiency measurement.

5. CONCLUSION

In summary, we have demonstrated bright telecom-wavelength single-photon sources based on In(Ga)As/GaAs QDs deterministically coupled to h-CBRs by using a wide-field fluorescence imaging technique. Single-photon purities of $g^{(2)}(0) = 0.11 \pm 0.02$ and $g^{(2)}(0) = 0.087 \pm 0.003$ can be achieved under low-power CW (0.2 μW) and pulsed (1.2 μW) excitations, respectively. The highest photon count rates of 1.14 MHz and 0.34 MHz with $g^{(2)}(0) = 0.38 \pm 0.03$ and $g^{(2)}(0) = 0.485 \pm 0.003$ are obtained at saturation powers for CW (4.8 μW) and pulsed (5.4 μW) excitations, respectively. The coupling between the QD and h-CBR is revealed by a Purcell factor of 4.2 and an improved first lens extraction efficiency of 11.2% ± 1%. Deviations of the measured device specifications from the numerical simulations can be ascribed to the spectral and spatial mismatches between the QDs and h-CBR, which could be further minimized in the future with technological efforts. Moving forward, more advanced designs with implementation of a PIN gate [47–49] could be exploited to stabilize the charge environment of the QDs, which may suppress the blinking behavior and enable the observation of resonance fluorescence for highly coherent single-photon emissions in the telecom band [31,50].

6. METHOD

Before fabricating the h-CBR structures, the sample was mounted in a cryostat (Montana) with an internally installed objective (NA = 0.65) and cooled down to about 4 K. For wide-field QD positioning, a CW laser with a wavelength at ~780 nm was used to excite the QDs, and an LED with a center wavelength at 1550 nm was used to illuminate the sample surface. By adding long pass filters of 900 nm and 1300 nm, fluorescence images of individual QDs and alignment Au marks were obtained on an infrared liquid-nitrogen-cooled InGaAs array detector (NIRvana-LN, Princeton Instruments). To remove the background noises caused by ambient light, a background image was taken before capturing the signal image. After fabricating the structures, the sample was tested by the same setup but turning the flip BS (BSW29R, Thorlabs) and flip mirror to the right sight (as seen in Fig. 5). The dichroscope (DM10-650LP, LBTEK) was replaced by a BS (BSW29R, Thorlabs) for clear imaging. The emission lines were coupled into a fiber and collimated in a spectrometer for spectral acquisition. With the help of the spectrometer, we can select the targeted emission line by a home-built filter setup (FWHM ~ 0.3 nm). A half-wave plate and a quarter-wave plate were used to improve the diffraction efficiency of the grating, which is polarization dependent. Then the filtered signal was divided by a fiber BS detected by two fiber-coupled SNSPDs with a dead time of 100 ns. Because the detection efficiency of the SNSPD was sensitive to the polarization of photons, a fiber polarization controller was used to turn the count rate to maximum.

Funding. National Key Research and Development Program of China (2018YFA0306103); Special Project for Research and Development in Key areas of Guangdong Province (2018B030329001); National Natural Science Foundation of China (11874437, 12074442, 62035017, 91836303); Guangdong Special Support Plan (2019JC05X397).

Acknowledgment. We acknowledge the National Supercomputer Center in Guangzhou.

Disclosures. The authors declare no conflicts of interest.

Data Availability. Data underlying the results presented in this paper are not publicly available at this time but may be obtained from the authors upon reasonable request.

[†]These authors contributed equally to this work.

REFERENCES

1. T. Chanelière, D. N. Matsukevich, S. D. Jenkins, T. A. B. Kennedy, M. S. Chapman, and A. Kuzmich, "Quantum telecommunication based on atomic cascade transitions," Phys. Rev. Lett. **96**, 093604 (2006).
2. J. Volz, M. Weber, D. Schlenk, W. Rosenfeld, J. Vrana, K. Saucke, C. Kurtsiefer, and H. Weinfurter, "Observation of entanglement of a single photon with a trapped atom," Phys. Rev. Lett. **96**, 030404 (2006).
3. S. Zaske, A. Lenhard, C. A. Keßler, J. Kettler, C. Hepp, C. Arend, R. Al-brecht, W.-M. Schulz, M. Jetter, P. Michler, and C. Becher, "Visible-to-telecom quantum frequency conversion of light from a single quantum emitter," Phys. Rev. Lett. **109**, 147404 (2012).
4. J. H. Weber, B. Kambs, J. Kettler, S. Kern, J. Maisch, H. Vural, M. Jetter, S. L. Portalupi, C. Becher, and P. Michler, "Two-photon interference in the telecom C-band after frequency conversion of photons from remote quantum emitters," Nat. Nanotechnol. **14**, 23–26 (2019).
5. V. Ustinov, N. Maleev, A. Zhukov, A. Kovsh, A. Y. Egorov, A. Lunev, B. Volovik, I. Krestnikov, Y. G. Musikhin, N. Bert, P. S. Kop'ev, Z. I. Alferov, N. N. Ledentsov, and D. Bimberg, "InAs/InGaAs quantum dot structures on GaAs substrates emitting at 1.3 μm," Appl. Phys. Lett. **74**, 2815–2817 (1999).
6. T. Miyazawa, K. Takemoto, Y. Nambu, S. Miki, T. Yamashita, H. Terai, M. Fujiwara, M. Sasaki, Y. Sakuma, M. Takatsu, T. Yamamoto, and Y. Arakawa, "Single-photon emission at 1.5 μm from an InAs/InP quantum dot with highly suppressed multi-photon emission probabilities," Appl. Phys. Lett. **109**, 132106 (2016).
7. B. Alloing, C. Zinoni, V. Zwiller, L. Li, C. Monat, M. Gobet, G. Buchs, A. Fiore, E. Pelucchi, and E. Kapon, "Growth and characterization of single quantum dots emitting at 1300 nm," Appl. Phys. Lett. **86**, 101908 (2005).
8. M. Benyoucef, M. Yacob, J. Reithmaier, J. Kettler, and P. Michler, "Telecom-wavelength (1.5 μm) single-photon emission from InP-based quantum dots," Appl. Phys. Lett. **103**, 162101 (2013).
9. J. Wang, Y. Zhou, Z. Wang, A. Rasmita, J. Yang, X. Li, H. J. von Bardeleben, and W. Gao, "Bright room temperature single photon source at telecom range in cubic silicon carbide," Nat. Commun. **9**, 4106 (2018).
10. L. Spindlberger, A. Csóré, G. Thiering, S. Putz, R. Karhu, J. Hassan, N. Son, T. Fromherz, A. Gali, and M. Trupke, "Optical properties of vanadium in 4H silicon carbide for quantum technology," Phys. Rev. Appl. **12**, 014015 (2019).
11. Z. Mu, A. Rasmita, J. Yang, X. Li, and W. Gao, "Room-temperature solid-state quantum emitters in the telecom range," Adv. Quantum Technol. **4**, 2100076 (2021).
12. X. He, N. F. Hartmann, X. Ma, Y. Kim, R. Ihly, J. L. Blackburn, W. Gao, J. Kono, Y. Yomogida, A. Hirano, T. Tanaka, H. Kataura, H. Htoon, and S. K. Doorn, "Tunable room-temperature single-photon emission at telecom wavelengths from sp3 defects in carbon nanotubes," Nat. Photonics. **11**, 577–582 (2017).
13. X. Ma, N. F. Hartmann, J. K. Baldwin, S. K. Doorn, and H. Htoon, "Room-temperature single-photon generation from solitary dopants of carbon nanotubes," Nat. Nanotechnol. **10**, 671–675 (2015).
14. X.-H. Bao, A. Reingruber, P. Dietrich, J. Rui, A. Dück, T. Strassel, L. Li, N.-L. Liu, B. Zhao, and J.-W. Pan, "Efficient and long-lived quantum

memory with cold atoms inside a ring cavity," Nat. Phys. **8**, 517–521 (2012).
15. J. McKeever, A. Boca, A. Boozer, R. Miller, J. Buck, A. Kuzmich, and H. Kimble, "Deterministic generation of single photons from one atom trapped in a cavity," Science **303**, 1992–1994 (2004).
16. C. I. Osorio, N. Sangouard, and R. T. Thew, "On the purity and indistinguishability of down-converted photons," J. Phys. B **46**, 055501 (2013).
17. P. Senellart, G. Solomon, and A. White, "High-performance semiconductor quantum-dot single-photon sources," Nat. Nanotechnol. **12**, 1026–1039 (2017).
18. X. Ding, Y. He, Z.-C. Duan, N. Gregersen, M.-C. Chen, S. Unsleber, S. Maier, C. Schneider, M. Kamp, S. Höfling, C.-Y. Lu, and J.-W. Pan, "On-demand single photons with high extraction efficiency and near-unity indistinguishability from a resonantly driven quantum dot in a micropillar," Phys. Rev. Lett. **116**, 020401 (2016).
19. N. Somaschi, V. Giesz, L. De Santis, J. Loredo, M. P. Almeida, G. Hornecker, S. L. Portalupi, T. Grange, C. Anton, J. Demory, C. Gómez, I. Sagnes, N. D. Lanzillotti-Kimura, A. Lemaítre, A. Auffeves, A. G. White, L. Lanco, and P. Senellart, "Near-optimal single-photon sources in the solid state," Nat. Photonics. **10**, 340–345 (2016).
20. Y.-M. He, J. Liu, S. Maier, M. Emmerling, S. Gerhardt, M. Davanço, K. Srinivasan, C. Schneider, and S. Höfling, "Deterministic implementation of a bright, on-demand single-photon source with near-unity indistinguishability via quantum dot imaging," Optica **4**, 802–808 (2017).
21. S. Liu, Y. Wei, X. Li, Y. Yu, J. Liu, S. Yu, and X. Wang, "Dual-resonance enhanced quantum light-matter interactions in deterministically coupled quantum-dot-micropillars," Light Sci. Appl. **10**, 158 (2021).
22. M. Davanco, M. T. Rakher, D. Schuh, A. Badolato, and K. Srinivasan, "A circular dielectric grating for vertical extraction of single quantum dot emission," Appl. Phys. Lett. **99**, 041102 (2011).
23. J. Liu, R. Su, Y. Wei, B. Yao, S. F. C. da Silva, Y. Yu, J. Iles-Smith, K. Srinivasan, A. Rastelli, J. Li, and X. Wang, "A solid-state source of strongly entangled photon pairs with high brightness and indistinguishability," Nat. Nanotechnol. **14**, 586–593 (2019).
24. B. Chen, Z. He, Z.-J. Liu, Y.-K. Wang, Y.-N. Gao, I. Aharonovich, Z.-Q. Xu, and J. Liu, "Simultaneously enhanced linear and nonlinear photon generations from WS_2 by using dielectric circular Bragg resonators," Nanophotonics **9**, 2587–2592 (2020).
25. N. M. H. Duong, Z.-Q. Xu, M. Kianinia, R. Su, Z. Liu, S. Kim, C. Bradac, T. T. Tran, Y. Wan, L.-J. Li, A. Solntsev, J. Liu, and I. Aharonovich, "Enhanced emission from WSe_2 monolayers coupled to circular Bragg gratings," ACS Photon. **5**, 3950–3955 (2018).
26. F. Liu, A. J. Brash, J. O'Hara, L. M. Martins, C. L. Phillips, R. J. Coles, B. Royall, E. Clarke, C. Bentham, N. Prtljaga, I. E. Itskevich, L. R. Wilson, M. S. Skolnick, and A. M. Fox, "High Purcell factor generation of indistinguishable on-chip single photons," Nat. Nanotechnol. **13**, 835–840 (2018).
27. M. Arcari, I. Söllner, A. Javadi, S. Lindskov Hansen, S. Mahmoodian, J. Liu, H. Thyrrestrup, E. H. Lee, J. D. Song, S. Stobbe, and P. Lodahl, "Near-unity coupling efficiency of a quantum emitter to a photonic crystal waveguide," Phys. Rev. Lett. **113**, 093603 (2014).
28. N. Tomm, A. Javadi, N. O. Antoniadis, D. Najer, M. C. Löbl, A. R. Korsch, R. Schott, S. R. Valentin, A. D. Wieck, A. Ludwig, and R. J. Warburton, "A bright and fast source of coherent single photons," Nat. Nanotechnol. **16**, 399–403 (2021).
29. M. Paul, F. Olbrich, J. Höschele, S. Schreier, J. Kettler, S. L. Portalupi, M. Jetter, and P. Michler, "Single-photon emission at 1.55 μm from MOVPE-grown InAs quantum dots on InGaAs/GaAs metamorphic buffers," Appl. Phys. Lett. **111**, 033102 (2017).
30. M. Paul, J. Kettler, K. Zeuner, C. Clausen, M. Jetter, and P. Michler, "Metal-organic vapor-phase epitaxy-grown ultra-low density InGaAs/GaAs quantum dots exhibiting cascaded single-photon emission at 1.3 μm," Appl. Phys. Lett. **106**, 122105 (2015).
31. M. Anderson, T. Müller, J. Skiba-Szymanska, A. B. Krysa, J. Huwer, R. M. Stevenson, J. Heffernan, D. A. Ritchie, and A. J. Shields, "Coherence in single photon emission from droplet epitaxy and Stranski–Krastanov quantum dots in the telecom C-band," Appl. Phys. Lett. **118**, 014003 (2021).
32. A. Musiał, P. Holewa, P. Wyborski, M. Syperek, A. Kors, J. P. Reithmaier, G. Sęk, and M. Benyoucef, "High-purity triggered single-photon emission from symmetric single InAs/InP quantum dots around the telecom c-band window," Adv. Quantum Technol. **3**, 1900082 (2020).
33. S. Kolatschek, C. Nawrath, S. Bauer, J. Huang, J. Fischer, R. Sittig, M. Jetter, S. L. Portalupi, and P. Michler, "Bright Purcell enhanced single-photon source in the telecom o-band based on a quantum dot in a circular Bragg grating," Nano Lett. **21**, 7740–7745 (2021).
34. J.-H. Kim, T. Cai, C. J. Richardson, R. P. Leavitt, and E. Waks, "Two-photon interference from a bright single-photon source at telecom wavelengths," Optica **3**, 577–584 (2016).
35. C.-M. Lee, M. A. Buyukkaya, S. Harper, S. Aghaeimeibodi, C. J. Richardson, and E. Waks, "Bright telecom-wavelength single photons based on a tapered nanobeam," Nano Lett. **21**, 323–329 (2020).
36. N. Srocka, A. Musiał, P.-I. Schneider, P. Mrowinski, P. Holewa, S. Burger, D. Quandt, A. Strittmatter, S. Rodt, S. Reitzenstein, and G. Sęk, "Enhanced photon-extraction efficiency from InGaAs/GaAs quantum dots in deterministic photonic structures at 1.3 μm fabricated by *in-situ* electron-beam lithography," AIP Adv. **8**, 085205 (2018).
37. L. Sapienza, M. Davanço, A. Badolato, and K. Srinivasan, "Nanoscale optical positioning of single quantum dots for bright and pure single-photon emission," Nat. Commun. **6**, 7833 (2015).
38. J. Liu, M. I. Davanço, L. Sapienza, K. Konthasinghe, J. V. De Miranda Cardoso, J. D. Song, A. Badolato, and K. Srinivasan, "Cryogenic photoluminescence imaging system for nanoscale positioning of single quantum emitters," Rev. Sci. Instrum. **88**, 023116 (2017).
39. X. Huang, R. Su, J. Yang, M. Rao, J. Liu, Y. Yu, and S. Yu, "Wafer-scale epitaxial low density InAs/GaAs quantum dot for single photon emitter in three-inch substrate," Nanomaterials **11**, 930 (2021).
40. N. Srocka, P. Mrowinski, J. Große, M. von Helversen, T. Heindel, S. Rodt, and S. Reitzenstein, "Deterministically fabricated quantum dot single-photon source emitting indistinguishable photons in the telecom o-band," Appl. Phys. Lett. **116**, 231104 (2020).
41. B. Yao, R. Su, Y. Wei, Z. Liu, T. Zhao, and J. Liu, "Design for hybrid circular Bragg gratings for a highly efficient quantum-dot single-photon source," J. Korean Phys. Soc. **73**, 1502–1505 (2018).
42. L. Rickert, T. Kupko, S. Rodt, S. Reitzenstein, and T. Heindel, "Optimized designs for telecom-wavelength quantum light sources based on hybrid circular Bragg gratings," Opt. Express **27**, 36824–36837 (2019).
43. M. Radulaski, M. Widmann, M. Niethammer, J. L. Zhang, S.-Y. Lee, T. Rendler, K. G. Lagoudakis, N. T. Son, E. Janzén, T. Ohshima, J. Wrachtrup, and J. Vučković, "Scalable quantum photonics with single color centers in silicon carbide," Nano Lett. **17**, 1782–1786 (2017).
44. C. Santori, M. Pelton, G. Solomon, Y. Dale, and Y. Yamamoto, "Triggered single photons from a quantum dot," Phys. Rev. Lett. **86**, 1502–1505 (2001).
45. A. V. Kuhlmann, J. Houel, A. Ludwig, L. Greuter, D. Reuter, A. D. Wieck, M. Poggio, and R. J. Warburton, "Charge noise and spin noise in a semiconductor quantum device," Nat. Phys. **9**, 570–575 (2013).
46. A. L. Efros and M. Rosen, "Random telegraph signal in the photoluminescence intensity of a single quantum dot," Phys. Rev. Lett. **78**, 1110–1113 (1997).
47. A. Barbiero, J. Huwer, J. Skiba-Szymanska, T. Müller, R. M. Stevenson, and A. J. Shields, "Design study for an efficient semiconductor quantum light source operating in the telecom C-band based on an electrically-driven circular Bragg grating," Opt. Express **30**, 10919–10928 (2022).
48. S. Ji, T. Tajiri, H. Kiyama, A. Oiwa, and S. Iwamoto, "Design of bull's-eye optical cavity toward efficient quantum media conversion using gate-defined quantum dot," Jpn. J. Appl. Phys. **60**, 102003 (2021).
49. H. Singh, D. Farfurnik, Z. Luo, A. S. Bracker, S. G. Carter, and E. Waks, "Optical transparency induced by a largely Purcell-enhanced quantum dot in a polarization-degenerate cavity," arXiv:2111.13653 (2021).
50. C. Nawrath, H. Vural, J. Fischer, R. Schaber, S. Portalupi, M. Jetter, and P. Michler, "Resonance fluorescence of single In(Ga)As quantum dots emitting in the telecom C-band," Appl. Phys. Lett. **118**, 244002 (2021).